Jurnal Teknologi

Full paper

Performance-based Pushover Cyclic Test For Innovative Prefabricated Hybrid Industrialised Building System Sub-Frame

Jing-Ying Wong[a*], Abdul Kadir Marsono[a], Masine Md. Tap[b], Chun-Chieh Yip[a]

[a]*Faculty of Civil Engineering, Universiti Teknologi Malaysia, 81310 UTM Johor Bahru, Johor, Malaysia*
[b]*Faculty of Mechanical Engineering, Universiti Teknologi Malaysia, 81310 UTM Johor Bahru, Johor, Malaysia*

[*]Corresponding author: jywong@live.com.my

Article history

Received :12 August 2014
Received in revised form :
8 December 2014
Accepted :15 March 2015

Graphical abstract

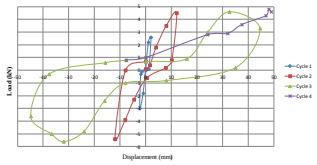

Abstract

The paper presents a pseudo-dynamic cyclic load test to evaluate the structural performance of innovative prefabricated hybrid Industrialised Building System (IBS) subjected to earthquake-induced ground motions. Two beams, three columns and six wall panels with scale of 1:5 were casted using concrete grade 30. Steel bars with diameters of 6 mm and 1.5 mm were used as main reinforcement and links, respectively. The frame was set-up and tested in two reversal directions of cyclic lateral loads in the structural laboratory. Eight Linear Variable Displacement Transducers (LVDTs) and seven strain gauges were instrumented in the model to record deflections and strains. This experiment was conducted in displacement-controlled mode. Four cycles of loads were applied corresponding to the initial targeted lateral displacement to obtain hysteresis curve. The structural performance was assessed using structural seismic demand parameters such as story displacement, displacement ductility and energy dissipation. Three structural performance levels that were Immediate Occupancy (IO), Life Safety (LS) and Collapse Prevention (CP) were assessed with compliance of FEMA 356. Structural behaviour, localised stressed and failed components were checked and recorded. The experimental results were presented in load-displacement of the system, mapped crack patterns, and development of capacity curve. Damage ranking were proposed based on degree of damage of scaled 1:5 of SMART IBS frame.

Keywords: Industrialised Building System (IBS); pushover pseudo-dynamic cyclic load test; hysteresis curve; capacity curve; damage ranking; damage index

Abstrak

Kertas ini membentangkan satu ujian beban kitaran pseudo-dinamik untuk menilai prestasi struktur hibrid pasang siap Sistem Binaan Berindustri (IBS) yang inovatif tertakluk kepada gerakan tanah disebabkan gempa bumi. Dua rasuk, tiga tiang dan enam panel dinding yang berskala 1: 5 telah diperbuat daripada konkrit bergred 30. Bar keluli dengan diameter masing-masing 6 mm dan 1.5 mm telah digunakan sebagai tetulang utama dan pautan. Kerangka telah dipasangkan dan diuji dalam dua arah pembalikan beban sisi kitaran dalam makmal struktur. Lapan Linear Pembolehubah Anjakan Transduser (LVDTs) dan tujuh tolok terikan telah dipasangkan ke dalam model untuk mencatatkan pesongan dan terikan. Eksperimen ini dijalankan dalam mod anjakan yang dikawal. Empat kitaran beban telah dijalankan sepadan dengan sasaran awal anjakan sisi untuk mendapatkan lengkung histerisis. Prestasi struktur telah dinilai dengan menggunakan parameter permintaan struktur seismik seperti anjakan tingkat, kemuluran anjakan dan pelesapan tenaga. Tiga tahap prestasi struktur iaitu Penghunian Segera (IO), Keselamatan Hayat (LS) dan Pencegahan Keruntuhan (CP) telah dinilai berdasarkan FEMA 356. Kelakuan struktur, tekanan setempat dan komponen yang gagal telah diperiksa dan dicatatkan. Keputusan eksperimen telah dibentangkan dalam sistem beban-anjakan, corak retakan, dan pembangunan lengkung kapasiti. Tahap kerosakan telah dicadangkan berdasarkan tahap kerosakan bingkai SMART IBS yang berskala 1: 5.

Kata kunci: Sistem Binaan Berindustri (IBS); ujian beban kitaran pseudo-dinamik; lengkung histerisis; lengkung kapasiti; tahap kerosakan; indeks kerosakan

1.0 INTRODUCTION

Industrialised Building Systems (IBS) is a construction process that utilises techniques, products, components, or building systems that involves prefabricated components and on-site installation [1]. It provides economisation of design, site work and materials. Zainal Abidin [2] describes that IBS is a construction method that offers economisation of design, site work and materials, provides shorter

construction time saving in labour, better quality control, immunity to weather changes and the cost factor.

In Malaysia, five major types of IBS based on structural aspects are precast reinforced concrete frame, panel and box system, steel formwork system, steel frame system, prefabricated timber frame system, and blockwork system [1]. However, the existing precast IBS is not designed to have a modular coordination system that can be assembled into various types of buildings in a short time.

The existing IBS cannot be mixed or inter-use, as they are not compatible to each other especially at its joints. They are manufactured and sold as separate systems due to their own unique designs. In addition, the systems are not specially designed to resist earthquakes, as they do not have a separation and decoupling of sub-assemblies.

IBS should be a transformable building. It should be designed for assembly, reconfigure, recycling and reuse. It can be changed, adapted, upgraded, or replaced based on user's preference as well as climate and geological conditions. All these criteria are attainable with SMART IBS, an internationally patented building system assembly [3].

SMART IBS is an open system that consists of integrated but inter-dependent sub-system to allow the change and addition of structural members based on user's demand to serve their purposes. Using the concept of modularization, which is modular in the dimensions of its components, the system can be transformed into various types of buildings such as single storey terrace house, shop terrace house, school and government building using the common SMART mechanical joint.

The SMART IBS system can also be expanded horizontally and vertically up to 6 storeys height because all the components are mountable and demountable. Hence, they can be in use longer as they can be adapted over time. In addition, it can be completed in a short time due to the introduction of pre-fabricated components to replace on-site works.

SMART IBS has separation and decoupling of sub-assemblies, which is the most important aspect for dynamic systems building. During an earthquake, the sub-assemblies will perform independently. As a result, the sub-assembly that fails will fail independently without affecting other sub-assembly. The failed sub-assembly can be disposed and then replaced within a short time and hence the user does not need to move out during the renovations.

In past years, earthquakes histories have revealed the poor performance of precast structures. Most of the structures did not survive through the severe seismic ground motions. They suffered excessive damages and collapsed eventually. Bournas *et al.* [4] stated that the main causes associated to the damage of the precast structures were failure of connections, insufficient ductility of the columns and insufficient stiffness of the roof or slab system. Five failure cases of precast structures are; 1976 Tangshan, China Earthquake [5], 1985 Michoacan, Mexico Earthquake [6], 1988 Spitak, Armenia Earthquake [7], 1994 Northridge, California Earthquake [8] and 1999 Kocaeli, Turkey Earthquake [9].

The seismic performances of SMART IBS need to be investigated to study its structural mode of failure and the connection's behaviour at the extreme maximum earthquakes lateral load capacity. The performance of SMART IBS is evaluated based on Federal Emergency Management Agency 356 (FEMA 356).

The research of SMART IBS was conducted previously by Moghadasi and Marsono [10]. Experimental study of patented full-scale H-subframe assembly was conducted for IBS reinforced concrete beam-to-column connection. Hence, further SMART IBS research was conducted and presented in this paper using pushover pseudo-dynamic cyclic load test.

Pushover analysis is a popular static nonlinear procedures in several seismic codes of ATC 40 [11], FEMA 273 [12], FEMA 356 [13], FEMA 440 [14], and SEAOC's Vision 2000 [15]. All these codes give detail guidelines on how to perform nonlinear static pushover analysis and seismic assessment. European Code 8 [16] stated that nonlinear static (pushover) analysis is a non-linear static analysis under constant gravity loads and monotonically increasing horizontal loads. Pushover analysis is a series of incremental linear, analysis that in each step, a portion of lateral load is applied to the structures [17].

Pushover analysis is response spectrum method of analysis. This analysis provides a fundamental relationship of base shear versus lateral displacement of the structure from elastic state to the ultimate failure and predicts the seismic demands on inelastic response of the structure.

Pushover analysis can be done in terms of force controlled or displacement controlled [18]. In the force control, the total lateral load is applied incrementally. The structure is analysed in elastic state until ultimate failure occurs. In the displacement control, the displacement at the top storey of the structure is incremented by lateral force. The displacement controlled pushover analysis is generally preferred than the force controlled because the analysis can be done accordingly to the target displacement.

The basic step of a pushover test was outlined by Tso and Moghadam [19]. Seismic demand on the building is by setting the target displacement is used to evaluate the damage potential of the building when subjected to a specific level of ground shaking. A target displacement is an estimation of the top displacement of the building when exposed to the specified level of ground shaking. Lateral force-displacement relationship is then obtained to represent system performance.

Vatansever and Yardimci [20] have demonstrated the cyclic behaviour and numerical modelling of a steel frame. Figure 1 shows the cyclic response of the specimen that is characterized by an open stable hysteretic behaviour superimposed on the push over curve from the numerical analysis. The load-deflection envelopes of the specimen for the pushing and pulling directions were plotted in Figure 2 to examine the load capacity and to compare the initial stiffness and the ultimate strength of the system.

A capacity curve represents the nonlinear behaviour of the system and its structural performance level. The capacity curve of the structure normally represents base-shear force versus top displacement relationship. It is evaluated by monotonically increasing the horizontal forces applied to the structure [21]. Bozorgnia and Bertero (Eds.) [22] defined that a point in this curve represents a damage state in the building as the deformation of all the structure components can be related to the control point displacement.

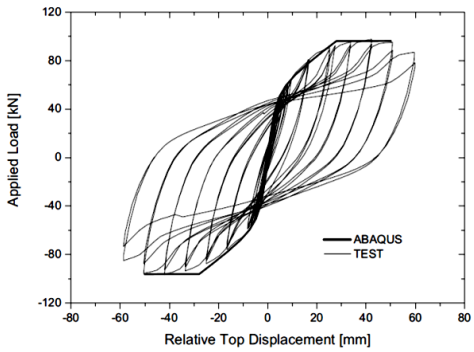

Figure 1 Hysteresis loops of the steel frame [20]

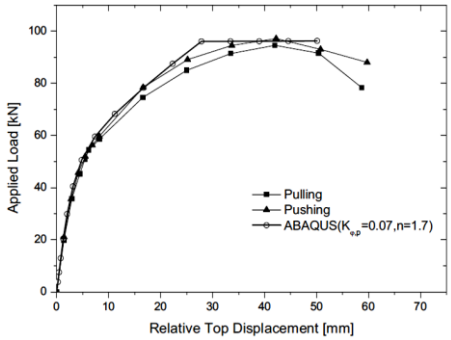

Figure 2 Envelopes of the steel frame in the pushing and pulling directions [20]

Figure 3 shows a relationship of typical lateral load versus roof displacement performance for a structure obtained from the pushover analysis by Ghobarah [23]. Performance of a building can be evaluated based on the expected damage levels of no damage, minor damage, moderate repairable damage, severe damage, and collapse. The sequence of component cracking, yielding and failure as well as the history of deformation of the structure can be traced as the lateral loads (or displacements) are monotonically increased.

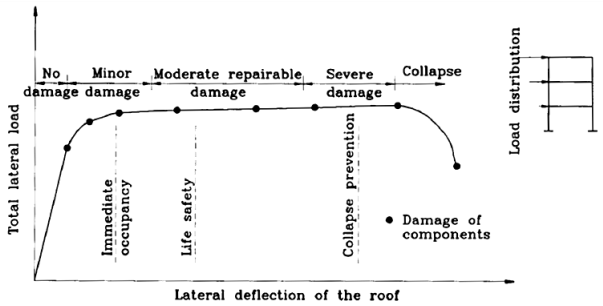

Figure 3 Typical performance curve from pushover analysis [3]

Several pushover experiments were conducted by various researchers, but the full-scale real life type structure is the best, due to its geometrically real behaviour under lateral seismic loading that revealed realistic and reliable results. Previously, Nakashima *et al.* [24] and Pinho and Elnashai [25] performed pushover tests on full-scale reinforced concrete structures. In addition, pushover loads were conducted by Weng *et al.* [26] and Tu *et al*. [27] on school building in Taiwan.

Wang *et al.* [28] carried out lateral cyclic loading to investigate hysteretic energy dissipation capacity and lateral strength of precast segment construction for tall concrete bridge columns.

An analytical study using the finite element method has also been used by researchers to study the bond conditions, strain contours and deformation patterns of test specimens. Zhang *et al.* [29] conducted numerical simulation and analysis of a pushover of a full scale two-story full-scaled dense column frame. The model was analysed using ABAQUS, SAP2000, and PKPM. The simulation result was compared with test data to verify the reliability of numerical method through pushover analysis method in evaluating the structures' seismic capacity.

Sharma *et al.* [30] presented experimental and numerical work of a full-scale four storey reinforced concrete (RC) structure for seismic assessment by pushover method.

These full scale experimentations carried out were costly as well as requiring excessive time and effort. Hence, in this paper, the performance of small-scale model of new prefabricated hybrid Industrialised Building System (IBS) [3] was evaluated. This research intends to investigate seismic demand on the building by controlled displacement cyclic lateral load test. The failure mechanism and crack patterns of 1:5 scaled model were assessed. Seismic demand parameters were obtained to determine the structural performance level.

■2.0 EXPERIMENTAL MODELS AND TEST SPECIFICATIONS

2.1 Structural Specifications

Two scaled 1:5 model of SMART IBS sub-frames were constructed and tested to investigate the structure performance of the model when subjected to cyclic lateral loads. The sub-frames consist of two beams, three columns and six wall panels.

The model's length of both beam and column was 660 mm to represent a distance of 3500 mm in the full scale residential housing structures. Both beam and column has 60 mm x 60 mm cross section. The concrete column has slot hole of 10 x 10 x 80 mm to provide connection for wall panels. Steel plate was used to connect the panel to the column. Steel rectangular hollow section (RHS) of 25 x 25 x 120 mm of column was connected to the U-shaped steel plate of 160 x 40 x 20 mm in the beam-ends by using bolt and nut.

The diameter of all reinforcements and links were 6 mm and 1.5 mm respectively. The concrete cover of 6 mm was provided to the main reinforcements. All the materials used for the small-scale model were based on availability of steel and concrete materials in the market. Figure 4 shows the specifications and details of the IBS frame formation.

The U-shaped steels plates were tied together with two 6 mm diameter longitudinal main reinforcements at top and bottom in the IBS beam. The half height of steel rectangular hollow section of column was casted together into the concrete to provide bond between the concrete and connectors.

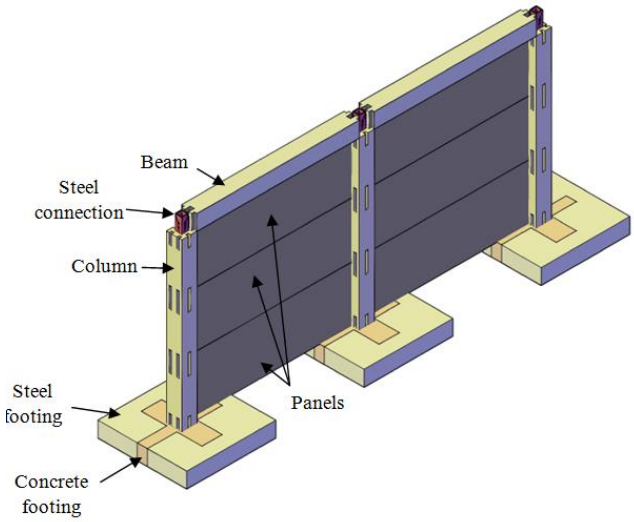

(a)

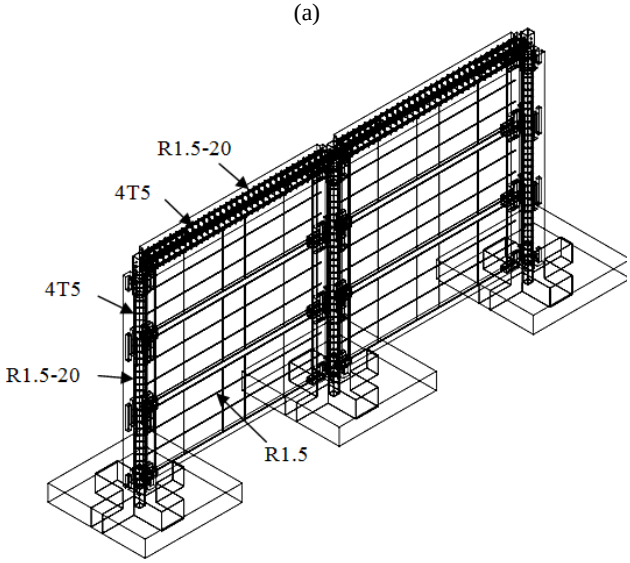

(b)

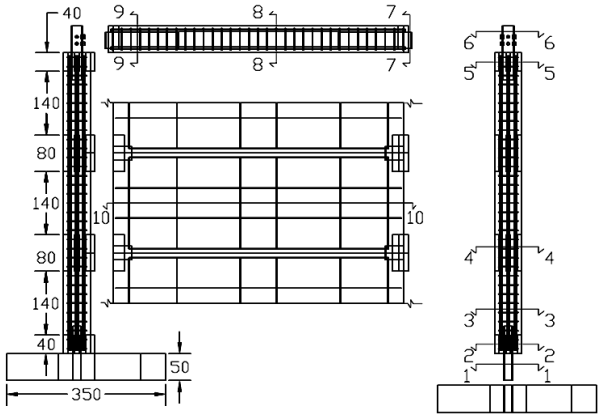

(c)

Figure 4 IBS model elevation view and details (Building Assembly System): (a) 3D perspective view; (b) 3D wireframe view; (c) 2D front view; (d) cross sections

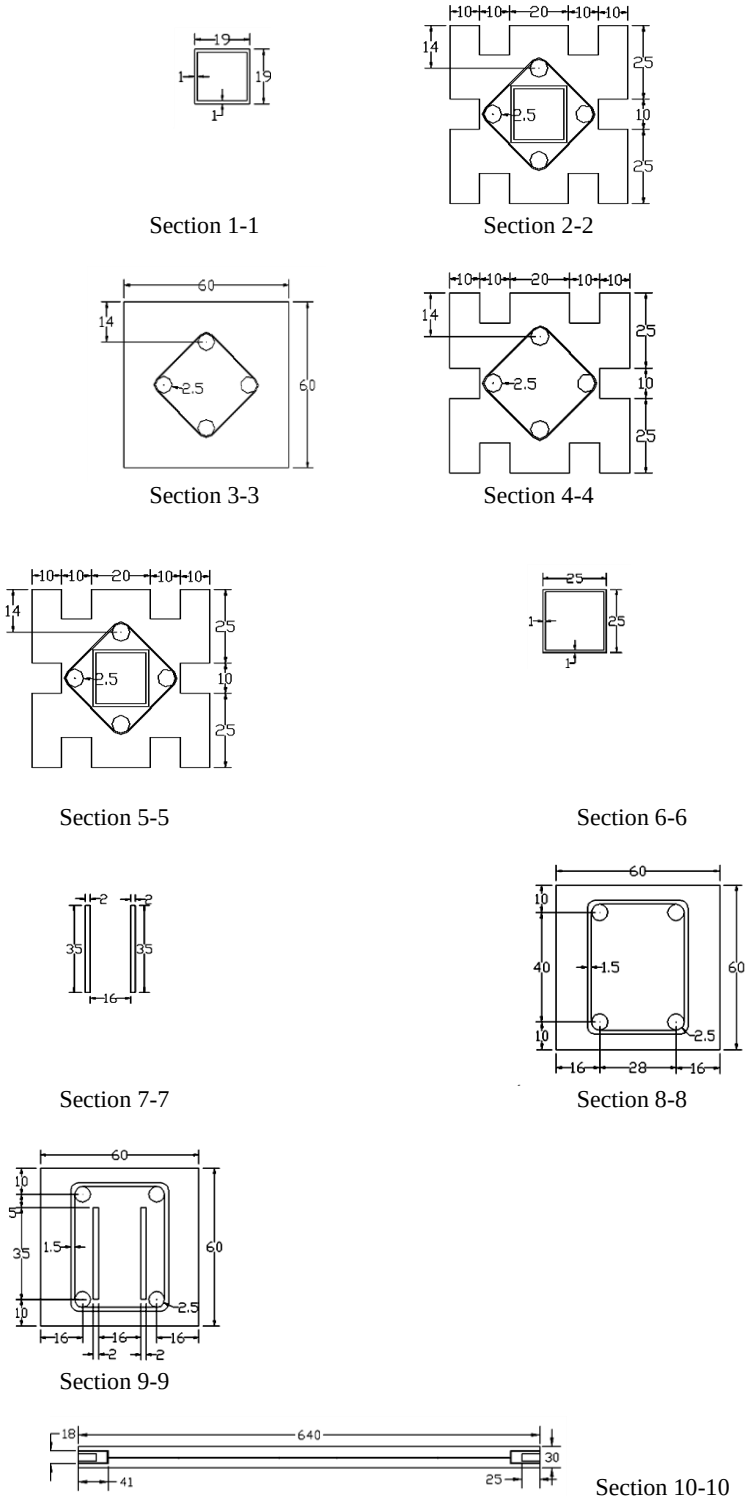

(d)

Figure 4 IBS model elevation view and details (Building Assembly System): (a) 3D perspective view; (b) 3D wireframe view; (c) 2D front view; (d) cross sections (continue)

2.2 Materials Properties

All the steels were tested in laboratory by Universal Testing Machine to obtain its mechanical properties. The main mechanical properties such as yield stress, yield strain, ultimate stress, ultimate strain and modulus of elasticity are shown in Table 1.

Table 1 Mechanical properties of steel

Type	Diameter/ Thickness (mm)		f_y	ε_y	f_u	ε_u	E
	Nominal	Measured	(MPa)	(%)	(MPa)	(%)	(GPa)
Steel (link)	1.5	1.52	922.74	0.60	964.57	1.44	227.343
Steel bar	5	5.38	650.70	0.32	761.99	1.46	199.578
Steel plate (panel)	1	0.64	819.57	0.57	822.87	0.64	223.060
Steel plate (column)	1	0.86	222.60	0.31	253.80	9.20	150.700
Steel plate (beam)	2	2.64	446.09	0.32	555.57	17.30	206.441

Notation: f_y and ε_y are yield strength and strain respectively while f_u and ε_u are ultimate strength and strain respectively

Concrete of grade 30 was used to cast the scale of 1:5 model. Control specimen of three cylinders of 100x200 mm were casted for every batch of casting and cured simultaneously together with the IBS components to obtain the representative compressive and tensile strength of the concrete. The tested mechanical properties of concrete were are shown in Table 2.

Table 2 Mechanical properties of concrete

Material	Characteristic Strength, f_{cu} (N/mm^2)	Compressive Strength, f_{cu} (N/mm^2)	Splitting Strength, f_t (N/mm^2)
Concrete	30	35.64	3.615

2.3 Loading Specifications

The steel footings were held rigidly at its surrounding to prevent the overturning or sliding of the footing. The concrete were casted into footing to fix permanently the end of RHS of the column. Eight Linear Variable Displacement Transducers (LVDTs) were installed on the frame. Three LVDTs were installed on the beam to measure its vertical deflection. Two LVDTs were installed on steel footing to ensure no footing movement during the test. Two LVDTs were installed at both ends of the frame to obtain the lateral displacement which also act to control the laterally induced movement. One LVDT was installed at one-third length of column from bottom to measure the column base deflection.

The localised responses were measured using electrical strain gauges glued on reinforcement bars and column RHS. The magnitude of lateral induced loads was measured using a load cell. After equipments were set, total load of 0.4 kN using steel blocks were imposed on both beams' clear span to act as a permanent dead and imposed load on the beams. Two steel bars were installed on the frame together with the transfer bar. The lateral cyclic load was applied pulling the model through the hydraulic jack horizontally.

The model was displaced horizontally in four cycles of loading and unloading in both lateral directions. Any cycle will be stop when the target displacement was achieved. For each cycle, the load was applied in several small incremental of displacement steps to predetermined levels. Each cycle was loaded according to the pre-calculated target displacement on structural performance level from FEMA 356 calculations. This procedure is not applied to the ultimate capacity test where the model was displaced up to failure in a single push. Figure 5 shows the test set-up of the system in laboratory.

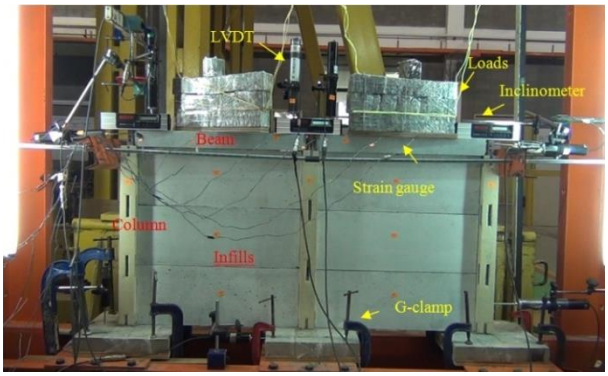

(a)

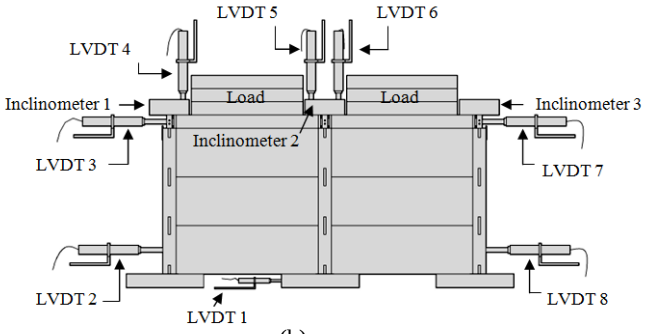

(b)

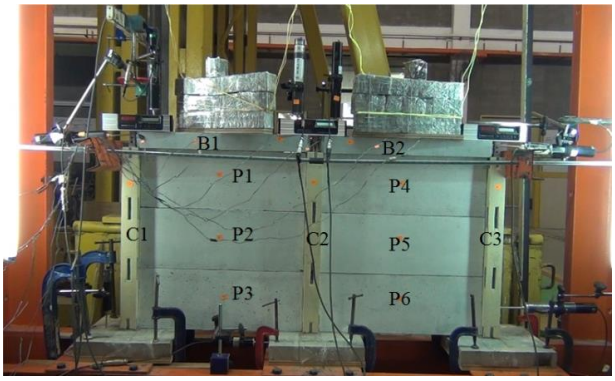

(c)

Figure 5 Test set-up of scale 1:5 sub-frame: (a) experimental set-up; (b) perspective view of set-up; (c) identity of components

Figure 5 Test set-up of scale 1:5 sub-frame: (a) experimental set-up; (b) perspective view of set-up; (c) identity of components (continue)

3.0 RESULTS AND DISCUSSION

3.1 Load-displacement of System

Figure 6 shows the hysteresis profile of frame assembly. Hysteresis profile was used to distinguish the degradation of strength and stiffness for nonlinear dynamic analysis. Under reverse cyclic loading, the frame apparently losses in strength under increasing deformations due to concrete cracking and crushing, shear failure, and bond slip.

Three performance levels that are Immediate Occupancy (IO), Life Safety (LS), and Collapse Prevention (CP) were identified in the experiment as compliance with FEMA 356. The initial stiffness in the first cycle of load represents the stiffness of structure at undamaged state. As the reversal displacement cycles were conducted, the initial stiffness at the beginning of each new cycle was degraded due to the damages from the previous loadings cycles. The strength and stiffness were observed to degrade after each cycle of load.

The first cycle of loading was conducted to detect the instance of the first crack that indicates the system was at the limit of serviceability limit state. The frame was essentially at fully elastic state and at performance level of IO since the system was detected to be able to return to its original position when all loads were released.

In the second cycle of loading, the frame was pushed to the limit of IO performance level. Some new minor hairlines and extended cracks were observed in columns and wall panels. This indicates that the frame starts to undergo the post-elastic process. In the third cycle of loading, the frame was in LS performance level at 32.63 mm displacement. Then, the frame reached CP performance level at the end of third cycle at 43.5 mm lateral displacement.

In the fourth cycle of loading, the frame was loaded until fail. The frame almost collapsed in this final cycle with increment of lateral displacement but decrement of taken load. This phenomenon was happening when the frame has lost its internal resistance to resist any additional lateral load.

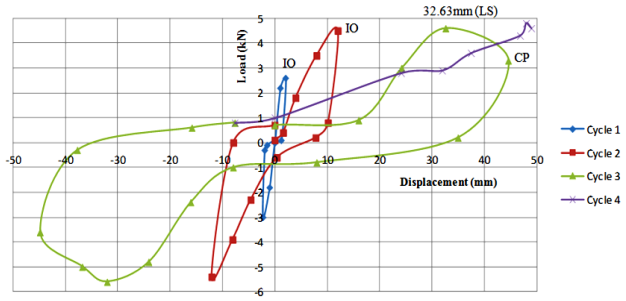

Figure 6 Hysteresis curve of frame

3.2 Crack Patterns and Mode of Failure

The sketch of crack pattern was coloured drawn to the model surface to identify the newly formed crack at the end of each loading cycle. The sketch was drawn for front and back view to simulate the global behaviour accurately. Photograph of the cracks pattern of every end cycle was taken as supporting evidence of the crack sketches and experiment.

Cracks describe the physical damages of structural elements of frame assembly due to the pseudo-dynamic cyclic lateral load test. The cracks length and width were measured to identify the state of structural performance level. Parameters such as material properties of reinforcing steel and concrete, cross section and sizes of components were affecting the failure modes and strength of its components.

Cycle 1

In this stage, the frame was loaded horizontally to 2.06 mm at load of 2.6 kN. Figure 7(a) shows the hysteresis curve obtained in cycle 1. The frame lateral displacement was increasing proportional to the value of load recorded. Then, the frame was return back to original position when it was fully unloaded. The frame was then loaded again to 2.29 mm of lateral displacement from the opposite direction and unloaded back to zero. The system again returned to its original position. This indicates that the frame was acting elastically in cycle 1 of loading.

A sketch of crack pattern of front and back view of the frame at the end of cycle 1 are shown in Figures 7(b) and (c). The photograph in Figure 7(d) was taken to conclude all the cracks and deformation of the frame.

Based on the assessment of frame, only some minor compressive cracks on panel surface were observed. Some minor cracks were observed at the slot connections of wall panel P1, P4 and P6. This was happening because when load was applied horizontally, the column is forced to move and push towards the panels, and this creates stress at the corner of panels. Wall panels were cracking because of the compressive force acting from the column. Insufficient gap between wall panel and column, and stiff of slot connection caused the part to crack. According to FEMA 356, the system was in Immediate Occupancy level since there is no permanent drift with minor overall damage. The structure retains its original stiffness since it can return to original position when it was fully unloaded.

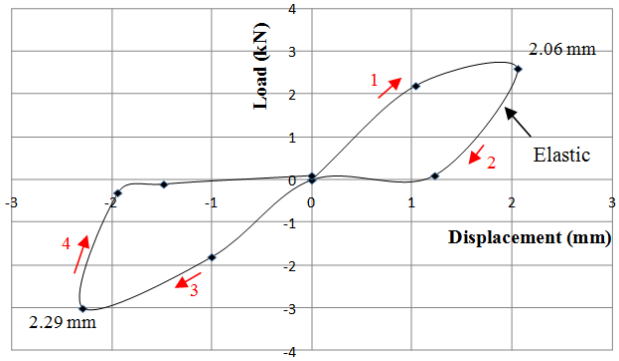

(a)

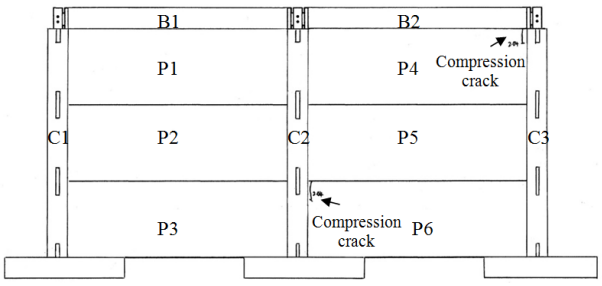

(b)

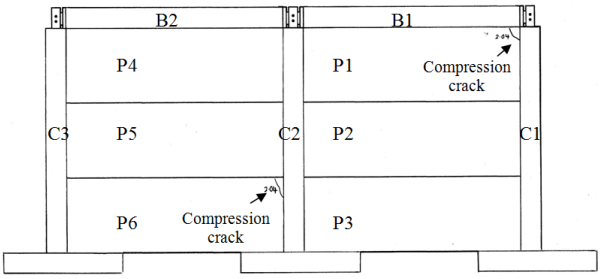

(c)

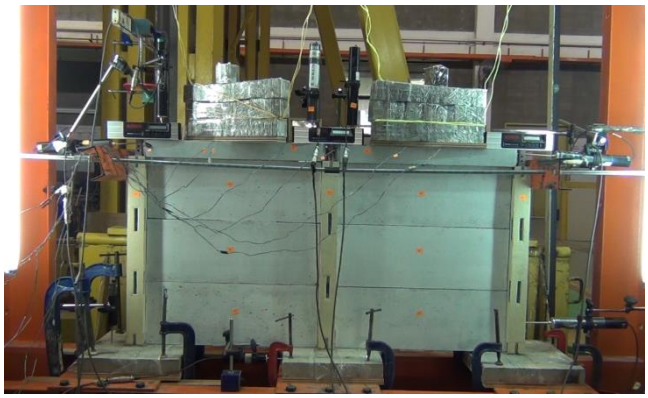

(d)

Figure 7 Cycle 1: (a) load - horizontal displacement relationship; (b) sketch of front view crack pattern; (c) sketch of back view crack pattern; (d) photograph

Cycle 2

In the second cycle, the frame was loaded horizontally to 12.05 mm with load of 4.5 kN. As the applied load was increasing, the frame displacement was also increasing. Then, the frame was unloaded after reaching the target displacement in second cycle. However, the frame had permanent drift of 7.83 mm when it was fully released from loaded stage. In this stage, the frame was not able to self-repositioning to its original state. Then, the jack was moved to the opposite side of the frame to jack the frame back to its original position. Hence, this condition can be observed in Figure 8(a) that an additional load was required in negative direction to push the frame from permanent drift of 7.03 mm back to its original position.

After the frame was loaded to its original position, the load was increased continually until lateral displacement of 12.03 mm with recorded 5.4 kN of resistance from load cell. Then, the frame was slowly unloaded. When the frame was fully unloaded, the frame has permanent drift of 7.89 mm as shown in Figure 8(a). This indicates that the frame has started to yield since the system was not able to return to original position in both directions.

A sketch of crack pattern of front and back view of the frame at the end of load cycle 2 were shown in Figures 8(b) and (c). The photograph in Figure 8(d) was taken to conclude all the cracks and deformation of the frame.

It was observed that the cracks originated at the corners of wall panels have propagated. Some newly visible narrow compressive cracks also appeared at the other corner of wall panels P2 and P3. Some visible minor flexural cracks with cracks width less than 0.2 mm were developed at the mid-span of column C1, C2 and C3. However, no crushing and spalling of concrete were observed at the end of cycle 2. The wall panels have some sliding at joints and separation of 2 mm from column. Hence, the system was in the limit state of Immediate Occupancy state.

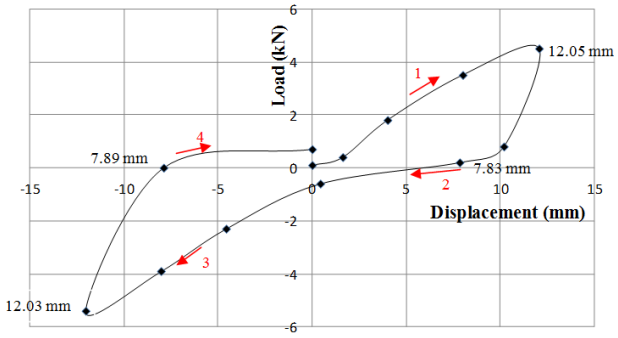

(a)

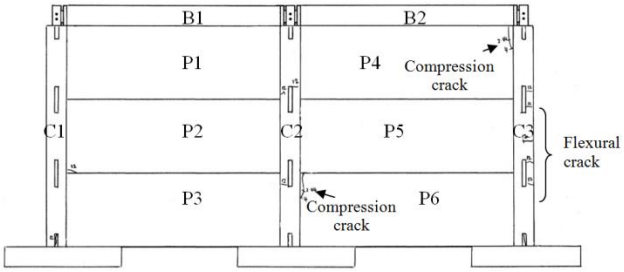

(b)

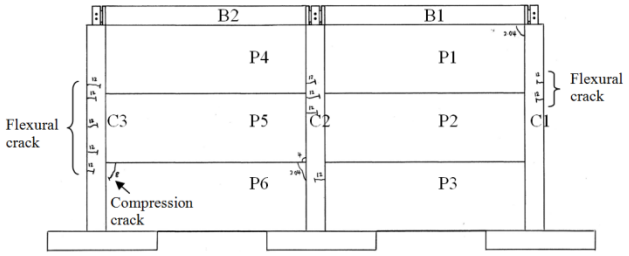

(c)

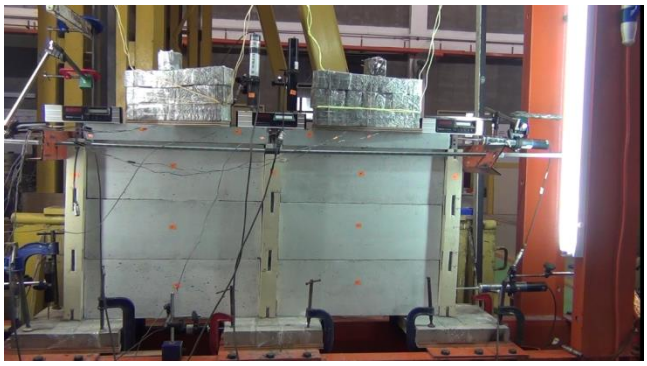

(d)

Figure 8 Cycle 2: (a) load - horizontal displacement relationship; (b) sketch of front view crack pattern; (c) sketch of back view crack pattern; (d) photograph

Cycle 3

In the third cycle, the frame was reloaded horizontally to target the displacement of 44.6 mm with load of 3.3 kN. Small increments of loads have caused the frame to displace drastically

at horizontal direction. The structure system has reached its maximum resistance capacity at lateral displacement of 32.63 mm with load of 4.6 kN. Then, the system starts to degrade with decrement of recorded load but increase of lateral displacement.

Then, the frame was slowly unloaded. However, the frame was permanently displaced at 34.99 mm when it was fully released from loaded state as shown in Figure 9(a). In this state, the frame was not able to self-reposition to original state. The jack was again moved to the opposite side of the frame set-up to jack the frame to its original position. This condition can be observed in Figure 9(a) that the additional load was required in negative direction to push the frame from permanent drift of 34.99 mm back to its original position.

After the frame was loaded to its original position, the load continues to be applied to the frame until the system meets its maximum resistance capacity on the opposite side direction. The maximum capacity of the system was at 33 mm with load 5.6 kN as shown in Figure 9(a). The system was degrading with decrement of recorded load and increase of lateral displacement. When the frame was fully released from loaded state, the frame had a permanent drift of 37.7 mm.

A sketch of the crack pattern of front and back view of the frame at the end of cycle 3 are shown in Figures 9(b) and (c). The photograph in Figure 9(d) was taken to conclude all the cracks and deformation of the frame.

At the 32.63 mm lateral displacement, some minor concrete spalling and visibly wide cracks were observed on the surface of wall panels P2 and P5. Column C2 and C3 have some visibly clear cracks and minor concrete spalling in this state.

At 44.6 mm lateral displacement, extensive concrete spalling were observed at the corner of wall panels P5 and P6 whereas minor spalling were observed at the corner of wall panel P1. The wall panels have some sliding at joints and is separated 5 mm from the column. Steel plate connections of wall panels P5 and P6 were exposed with extensive concrete spalling. The wall panels can be concluded as damaged components in this state.

Flexural cracks at the mid-span of columns C1, C2 and C3 have propagated with cracks width greater than 2 mm. In addition, the wide shear cracks have also propagated upward from bottom column and propagated downward from top of the column. The wide cracks cause the separation of RHS from column core concrete. At the end of the third cycle of test, the column C3 has uplifted 25 mm from footing. Based on the visual assessment, the system was in Collapse Prevention level as the column suffered major damage.

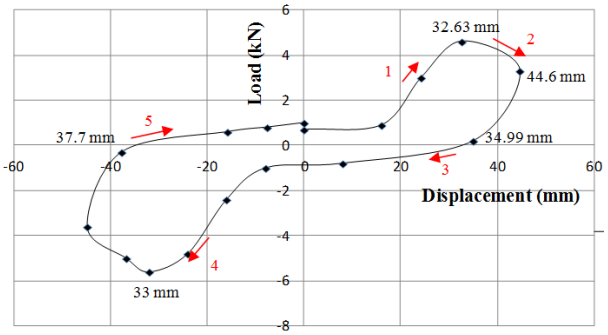

(a)

Figure 9 Cycle 3: (a) load - horizontal displacement relationship; (b) sketch of front view crack pattern; (c) sketch of back view crack pattern; (d) photograph

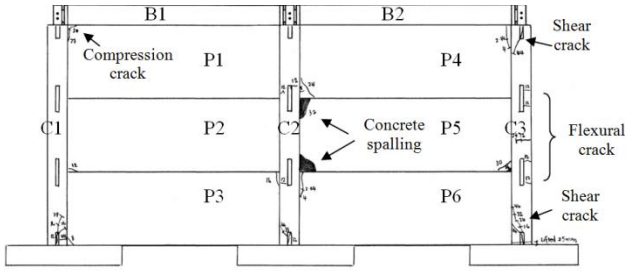

(b)

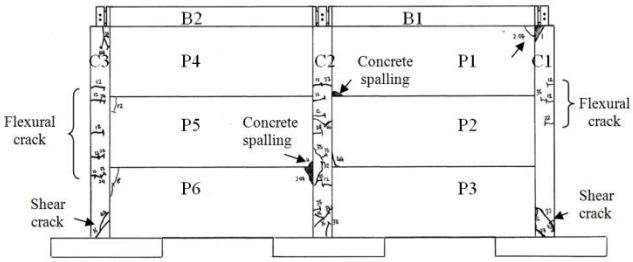

(c)

(d)

Figure 9 Cycle 3: (a) load - horizontal displacement relationship; (b) sketch of front view crack pattern; (c) sketch of back view crack pattern; (d) photograph (continue)

Cycle 4

In the last cycle, the frame was loaded horizontally until a complete failure occurred. As the frame was loaded, the displacement keeps on increasing. The system reached its maximum capacity at lateral displacement of 48 mm with load 4.8 kN before collapse as shown in Figure 10(a).

A sketch of crack pattern of front and back view of frame at the end of cycle 4 are shown in Figures 10(b) and (c). The photograph in Figure 10(d) was taken to conclude all the cracks and deformation of the frame.

In this cycle, wall panels P4, P5 and P6 have an extensive concrete crushing and spalling whereas wall panel P1 has minor concrete spalling. Hence, steel plates of connection of wall panels P4, P5 and P6 were exposed. Large pieces of panel concrete fell off during the experiment. The wall panel P2 was separated from column by 13.17 mm. Wall panels P5 and P6 were separated from each other vertically by 15.12 mm.

Flexural cracks at the mid-span of columns C1, C2 and C3 have propagated and crushing of core of concrete C1 was observed. With further additional load, the core concrete at the bottom of the column has crushes in the compression zone. The crushing of column core concrete causes the separation of RHS

from concrete. This induced the column to become unstable and hence the frame was in critical situation. The system was in earthquake Collapse Prevention level and then collapse without additional load. The experiment was stopped since the system almost collapsed as shown in Figure 10(d).

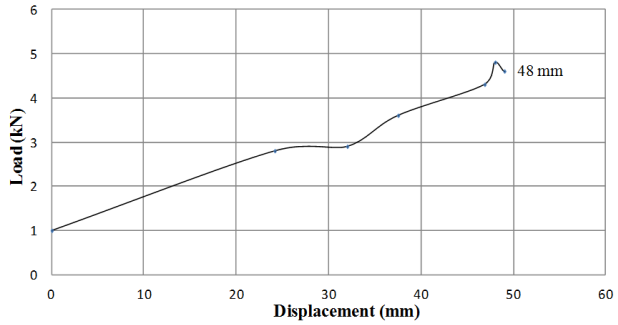

(a)

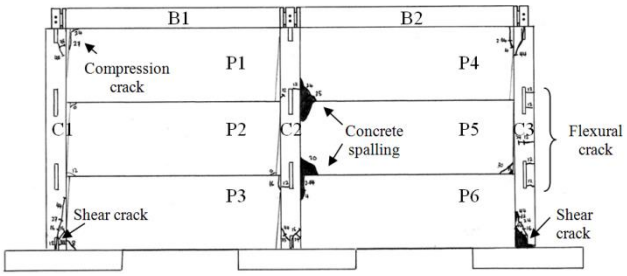

(b)

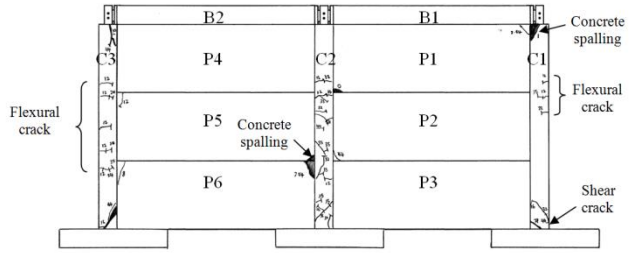

(c)

(d)

Figure 10 Cycle 4: (a) load - horizontal displacement relationship; (b) sketch of front view crack pattern; (c) sketch of back view crack pattern; (d) photograph

3.3 Deformation of Steel Connection

Three steel strain gauges were installed vertically inside RHS of column to detect local deformation of connection during the test. Figure 11 shows the load-strain curve of column RHS at the connection part. The recorded maximum strain of RHS was 1133 micro-strain (με) which was less than yield strain of RHS (0.0031). This shows the RHS of column was not yielding during the test.

This criterion is important for the IBS earthquake resistant structure. The failure of structural components before the failure of connection can prevent the catastrophic failure. If the connection fails before the structural components fails, then the beams and slabs will fall and cause massive casualties. After the test, the frame was dissembled and inspected. The damaged tracks of bolts indicate the stresses were transferred to the other components during the experiment.

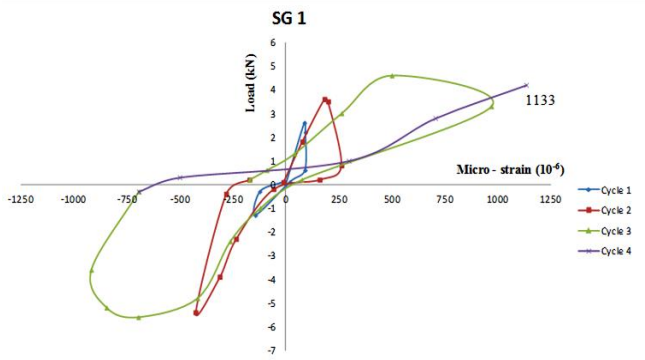

Figure 11 Load-strain curve of column RHS at connection part

3.4 Capacity Curve

Capacity curve was obtained by normalising the hysteresis curve in positive and negative direction as shown in Figure 12. This curve represents the system performance in linear and nonlinear state. Three performance levels that are Immediate Occupancy (IO), Life Safety (LS), and Collapse Prevention (CP) were identified in this experiment. The performance level of the system was determined through the damage experienced by the components. In short, it was measured based on damage intensity suffered by the system in compliance with FEMA 356.

In IO level, the structure achieves essentially elastic behaviour by limiting structural damages to light damages. Minor cracks occured at the corner part of wall panels while columns have minor hairline flexural cracks and no damage occurs in any other components.

In LS level, the overall damage of structure was rated as medium damage. There was some permanent drift occurred in the whole system. The wall panels have extensive concrete crushing and spalling at the corner parts. The columns have minor concrete spalling and extensive of shear cracks.

In CP level, the structure was ensured to have a small risk of partial or complete building collapse by limiting structural deformations and forces to the onset of significant strength and stiffness degradation. In this level, the overall structure has heavy damages. Large permanent drift was found in the system. Wall panels have an extensive concrete crushing and spalling at the corner parts that caused the exposure of steel plate connections. The wall panels were separated from column at connection part by 13.17 mm and separated from the other wall panels by 15.12 mm vertically. Columns have extensive concrete crushing at the

bottom parts that cause exposure of RHS, extensive flexural cracks at the mid-span of column, and concrete spalling at top and bottom parts of columns.

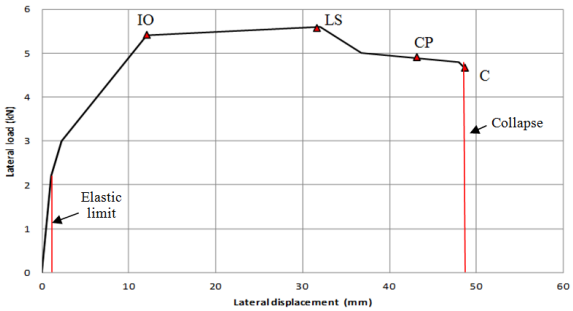

Figure 12 Capacity curve of frame

3.5 Structural Stiffness Capacity

Figure 13 shows the structural stiffness capacity curve and idealized bilinear curve. In elastic state, the structure has elastic lateral stiffness, K_i of 2.4 kN/mm. The recorded maximum base shear, V_t was 5.6 kN with story drift, δ_t of 32 mm. The bilinear curve was drawn to calculate the structural effective lateral stiffness, K_e and structural post-yield stiffness capacity, αK_e. It was drawn based on equal energy rule as the area above and below the curve was approximate balance.

The effective lateral stiffness, K_e was taken as secant stiffness calculated at a base shear force equal to 60% of the effective yield strength of the structure. The effective yield strength of the structure, V_y was 4.7 kN. The calculated effective lateral stiffness, K_e and structural post-yield stiffness capacity, αK_e were 1.34 kN/mm and 0.03 kN/mm respectively. This means the structure has stiffness degradation after it reached its yield state.

Stiffness degradation has the effect of reducing dissipated energy because the area under the load-displacement curve tends to decrease. As a result, the response of the structure becomes larger. The stiffness degradation of the frame was attributable to concrete crushing or spalling, and concrete-steel bond degradation.

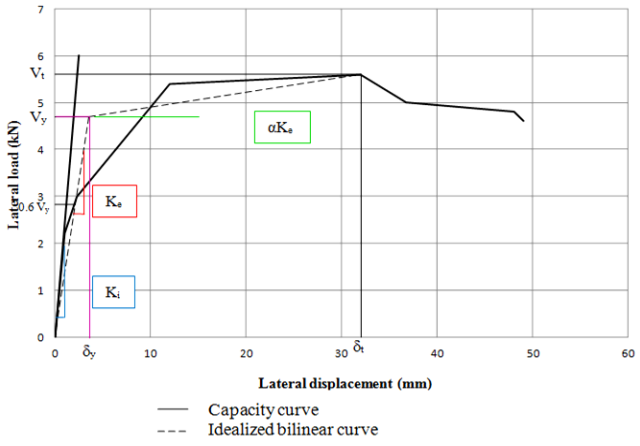

Figure 13 Initial and effective stiffness of frame

3.6 Structural Displacement Ductility and Energy Dissipation

System displacement ductility and energy dissipation are the important characteristics of a structure built to withstand earthquake loads. The ductility displacement of concrete structure ensures the sufficient deformability and avoids premature failure in either tension or compression zone.

The displacement ductility, μ is defined as the ratio of the maximum displacement attained at any cycle to the yield displacement. Ultimate displacement ductility, μ_u is defined as the displacement ductility when the system is considered to fail.

The energy dissipated per cycle of load is defined as the area enclosed by the load-displacement graph. The energy is dissipated through the inelastic deformations in a structure at various cyclic load reversals. Table 3 shows the system displacement ductility and energy dissipated per cycle of loads.

Figures 14 and 15 show the system displacement ductility and dissipated energy per cycle of loads respectively. In elastic state, both displacement ductility and dissipated energy were increasing as the load was increasing from load cycle 1 to load cycle 2 as shown in Figures 14 and 15. In load cycle 1 and 2, the frame has displacement ductility of 0.17 mm/mm and 1.0 mm/mm respectively. The frame was also dissipating the energy of 2.875 kN.mm and 26.875 kN.mm in the load cycle 1 and 2 respectively. It was observed that no damage occurred up to the yield displacement (end of load cycle 2).

However, the frame displacement ductility and dissipated energy were observed to increase drastically from load cycle 2 to load cycle 3 without much increment of loads. This was because the frame starts to yield at the end of load cycle 2. In load cycle 3, the nonlinear behaviour of frame starts to control the system and hence the frame continues to show the ductility and dissipate more energy by undergoing higher lateral displacement without much increase in the load. In load cycle 3, the frame has displacement ductility of 2.74 mm/mm and dissipated energy of 118.625 kN.mm.

In the load cycle 4, the frame starts to degrade with decrement of recorded load but increasing in lateral displacement. This indicates that the frame has lost its internal resistance to resist an additional lateral load. In load cycle 4, the frame has displacement ductility of 3.99 mm/mm and dissipated energy of 132.25 kN.mm. The ultimate displacement ductility of the frame was 3.99 mm/mm. In this state, the frame shows the highest lateral displacement of 48 mm before collapse. The total energy dissipation of the frame was 280.625 kN.mm.

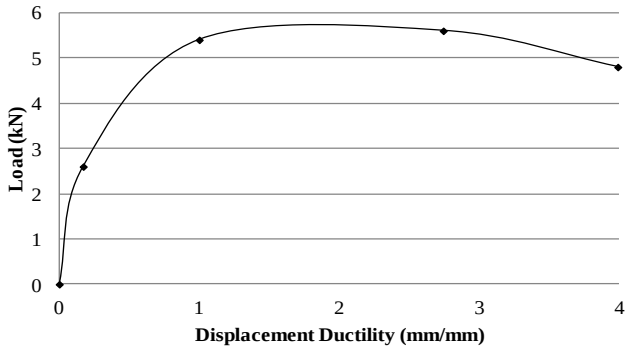

Figure 14 Graph of load versus displacement ductility

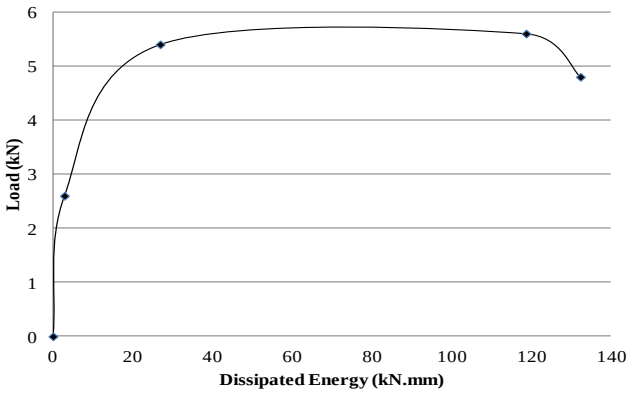

Figure 15 Graph of load versus dissipated energy

3.7 Proposed Damage Ranking

Damage ranking is proposed based on degree of damage of scaled 1:5 of SMART IBS frame. The damage descriptions of components for proposed damage ranking were shown in Table 4. The concept of the damage ranking is based on the similar approach by Okada and Takai [31] and Takashi *et al.* [32].

Table 3 System displacement ductility and energy dissipated per cycle of loads

Cycle No.	Load (kN)	Lateral displacement (mm)	Displacement Ductility (mm/mm)	Energy dissipated (kN.mm)	Cumulative energy dissipated (kN.mm)
1	2.6	2.06	0.17	2.875	2.875
2	5.4	12.03	1.0	26.875	29.75
3	5.6	33	2.74	118.625	148.375
4	4.8	48	3.99	132.25	280.625

Table 4 Damage descriptions of components for proposed damage ranking of SMART IBS

Damage Rank	Column	Beam	Panel
Rank 1 Slight	No shear cracks	No shear cracks (Crack width < 0.2 mm)	No shear cracks
Rank 2 Light	Visibly narrow shear cracks (Crack width < 0.2 mm)	Visibly clear shear cracks (crack width <1 mm)	Visibly narrow shear cracks
Rank 3 Medium	Visibly clear and/or wide shear cracks (0.2 < crack width < 2 mm) Minor spalling	Wide or big cracks (1< crack width < 5 mm) Local crush of cover concrete and small exposure of reinforcing bars	Minor spalling of concrete Visibly wide shear cracks
Rank 4 Heavy	Big cracks (Crack width >2 mm) Spalling of cover concrete Exposure of reinforcing bars without buckling Separation of RHS from concrete	Big shear cracks (Crack width > 5 mm) Extensive spalling of cover concrete Extensive exposure of reinforcing bars	Extensive spalling of concrete Some crushing and flexural cracking Separation of panel from column/ sliding at joints
Rank 5 Collapse	Crush of core concrete Extensive spalling in column Buckling and/or breaking of reinforcing bars	Crush of core concrete Buckling and/or breaking of reinforcing bars	Major flexural and shear cracks and voids Extensive crushing and buckling of reinforcement Buckling of steel plate Sliding at joints

4.0 CONCLUSION

This paper presented performance-based pushover cyclic test of small scale 1:5 prefabricated hybrid Industrialised Building System (IBS) sub-frame. From the results obtained, several conclusions can be drawn.

i. The structure was assessed based on three different performance levels, they are Immediate Occupancy (IO), Life Safety (LS) and Collapse Prevention (CP) in compliance with FEMA 356. The frame was in IO in cycle 1 and 2. At the end of cycle 2, the frame starts to yield. The frame was in LS state in cycle 3 up to displacement of 32 mm. Then, the frame was in state of CP until end of last cycle.

ii. In IO level, the structure was allowed to drift up to 3% laterally with no permanent drift. The displacement ductility demand and energy dissipation demand was 1.0 mm/mm and 26.875 kN.mm respectively. This means that beyond displacement ductility of 1.0 mm/mm, the structure was tending to behave plastically. The structure has ability to dissipate the energy up to 26.875 kN.mm through the deformations of structure and retains its original function. In this performance level, the structure retains its original strength and stiffness. The structure was back to function as normal system.

iii. In LS level, the structure was allowed to drift up to 4.71% laterally with some permanent drift. The displacement ductility demand and energy dissipation

demand was 2.74 mm/mm and 118.625 kN.mm respectively. This means that the nonlinear behaviour of structure starts to control the system and hence the structure continues to show the ductility and dissipated more energy by undergoing higher lateral displacement without much increase in the load. In this performance level, some residual strength and stiffness was left in the structure. The structure was beyond economical repair after earthquake.

iv. In CP level, the structure drifted more than 6.21% with permanent drift. The maximum displacement ductility demand and energy dissipation demand was 3.99 mm/mm and 132.25 kN.mm respectively. This means that the structure was achieving a ductile failure mode and has the ability to undergo relatively large inelastic deformations. In this performance level, little residual stiffness and strength was retained in the structure before collapse.

v. Five damage ranks (1 - 5) were proposed based on five damage index ranging from 0 to 1. The proposed damage ranks were based on damage intensity of the components and structural performance level. The damage descriptions of components for five proposed damage ranks and damage states was shown in Table 4 The proposed five damage states were Slight, Light, Medium, Heavy and Collapse. The assessment of the structure is based on three structural performance levels of Immediate Occupancy, Life Safety and Collapse Prevention.

Acknowledgement

This research was supported by UTM-URG-QJ130000.2522.05H06, Elastic Infills, Beams and Column for Natural Disaster Home.

References

[1] CIDB. 2003. *Industrialised Building System (IBS) Roadmap 2003-2010.* In CIDB. Malaysia (Ed.). Kuala Lumpur: CIDB.

[2] Zainal Abidin, A. R. 2007. *Simulation of Industrialised Building System Formation For Housing Construction.* Master of Science, Universiti Teknologi Malaysia, Johor, Malaysia.

[3] Building Assembly System. 2011. *International Patent No: PCT/MY2011/000182 PI2010003779.* Dr. Abdul Kadir Marsono, Dr. Ahmad Mahir Makhtar and Dr. Masine Md. Tap.

[4] Bournas, D. A., Negro, P. and Taucer, F. 2013. The Emilia Earthquakes: Report and Analysis on the Behavior of Precast Industrial Buildings from a Field Mission. *4th ECCOMAS Thematic Conference on Computational Methods in Structural Dynamics and Earthquake Engineering*. 12–14 June. Kos Island, Greece.

[5] Housner, G. W. and He, D. X. 2002. *Report on The Great Tangshan Earthquake of 1976.* California Institute of Technology. Pasadena, California.

[6] Girty, G. H. 2009. *Perilous Earth: Understanding Processes Behind Natural Disasters*. Department of Geological Sciences, San Diego State University.

[7] 1988. Death Toll Rises in Armenian Earthquake. December 10. *BBC News.*

[8] Lew, H. S., Cooper, J., Hays, W. and Mahoney, M. 1994. The January 17, 1994, Northridge Earthquake California. *National Institute of Standards and Technology (NIST) SP* 871. 375–426.

[9] Murat, S., Denis, M., Rene, T., N. John, G., Anthony, G. G. and Ahmed, G. 2001. The August 17, 1999, Kocaeli (Turkey) Earthquake -Damage to Structures. *Canada Journal Civil Engineering.*

[10] Moghadasi, M and Marsono, A. K. 2012. Comparative Experimental Study of Full-scale H-Subframe Using a New Industrialized Building System and Monolithic Reinforced Concrete Beam-to-Column Connection. *The Structural Design of Tall and Special Building*. Published online in Wiley Online Library.

[11] Applied Technology Council. 1996. *ATC 40*. California: Applied Technology Council.

[12] Federal Emergency Management Agency. 1997. *FEMA 273*. Washington: Applied Technology Council.

[13] Federal Emergency Management Agency. 2000. *FEMA 356*. Washington: American Society of Civil Engineers.

[14] Applied Technology Council. 2005. *FEMA 440.* Washington: Applied Technology Council.

[15] Vision 2000. 1995. Performance Based Seismic Engineering of Buildings. Structural Engineers Association of California. California.

[16] British Standard Institution. 2004. (Eurocode 8). London: British Standard Institution. BS EN 1998–1:2004

[17] Marsono, A. K and Khoshnoud, H. R. 2010. Evaluating Equivalent Static Analysis of Iranian Code with Nonlinear Static Pushover Analysis. *Proceedings of First Makassar International Conference on Civil Engineering (MICCE 2010*). Makassar, Indonesia.

[18] Datta, T. K. 2010. *Seismic Analysis of Structures*. Singapore: John Wiley & Sons (Asia) Pte Ltd.

[19] Tso, W. K. and Moghadam, A. S. 1998. Pushover Procedure for Seismic Analysis of Buildings. *Progress in Structural Engineering and Materials.* I(3): 337–344.

[20] Vatansever, C. and Yardimci, N. 2010. Cyclic Behavior and Numerical Modelling of a Semi-rigid Frame. *Steel Construction*. 3(3).

[21] Bosco, M., Ghersi, A. and. Marino, E. M. 2009. On the Evaluation of Seismic Response of Structures by Nonlinear Static Methods. *Earthquake Engineering & Structural Dynamics*. 38: 1465–1482.

[22] Bozorgnia, Y. and Bertero, V. V. (Eds.). 2004. *Earthquake Engineering-From Engineering Seismology to Performance-Based Engineering*. London: CRC Press.

[23] Ghobarah, A. 2000. Seismic Assessment of Existing RC structures. *Progress in Structural Engineeering and Materials.* 2: 60–71.

[24] Masayoshi Nakashima, Tomohiro Matsumiya, Keichiro Suita and Dawei Liu. 2006. Test on Full-scale Three Storey Steel Moment Frame and Assessment of Ability of Numerical Simulation to Trace Cyclic Inelastic Behaviour. *Earthquake Engineering & Structural Dynamics*. 35: 3–19.

[25] Pinho, R. and Elnashai, A. S. Dynamic Collapse Testing of a Full-scale Four Storey RC Frame. *ISET. Journal of Earthquake Technology* 2000. 37(4): 143–63.

[26] Weng, Y. T., Lin, K. C. and Hwang, S. J. 2006. Experimental and Analytical Performance Assessment of In-situ Pushover Tests of School Buildings in Taiwan. *4th International Conference on Earthquake Engineering.* Paper No. 154.

[27] Tu, Y. H., Jiang, W. C. and Hwang, S. J. 2006. In Situ Pushover Test of a School Building In Taiwan. *NCREE Newslett*er. 1(1).

[28] Wang, J. C., Ou, Y. C., Chang, K. C. and. Lee, G. C. 2008. Large-scale Seismic Tests of Tall Concrete Bridge Columns with Precast Segmental Construction. *Earthquake Engineering & Structural Dynamics.* 37: 1449–1465.

[29] Zhang, Y., Liu, J. J. and Qian, J. R. 2011. Numerical Simulation and Analysis of a Pushover of a Full-scale Two-story Model. *International Conference on Information Science and Technology*. March 26-28, Nanjing, Jiangsu, China.

[30] Sharma, A., Reddy, G. R., Vaze, K. K. and Eligehausen, R. 2013. Pushover Experiment and Analysis of a Full Scale Non-seismically Detailed RC Structure. *Engineering Structures*. 46: 218–233

[31] Okada, S. and Takai, N. 2000. Classification of Structural Types and Damage Patterns of Buildings for Earthquake Field Investigation. *12th World Conference on Earthquake Engineering*. 30 January-4 February. Auckland, New Zealand.

[32] Takashi, K., Fumitoshi, K. and Yoshiaki, N. 2002. *Quick Inspection Manual For Damaged Reinforced Concrete Buildings Due To Earthquakes: Based On Disaster Of 1999 Kocaeli Earthquake In Turkey.* National Institute of Land and Infrastructure Management.